



NEW ZEALAND SOCIETY FOR EARTHQUAKE ENGINEERING  
**2019 Pacific Conference on  
Earthquake Engineering**  
TURNING HAZARD AWARENESS INTO RISK MITIGATION  
4 – 6 April | SkyCity, Auckland | New Zealand



---

# Experimental testing and analytical modelling of grooved dissipaters

*M. Mashal*

Idaho State University, Idaho, United States

*A. Palermo*

University of Canterbury, Christchurch

## ABSTRACT

Grooved dissipaters are mini plug and play devices that can be used to dissipate seismic energy through axial deformation. In a grooved dissipater, a plain mild steel bar is used inside an outer confining tube. There are several cuts (grooves) made along the length of the bar where yielding occurs. There is a small gap (less than 1 mm) left between the tube and the bar. When the dissipater is in tension or compression, it yields from the machined (grooved) region. The outer confining tube prevents buckling of the dissipater under compression. Grooved dissipaters offer advantages such as easy fabrication, lower cost, higher strength, good ductility, and compactness. They were implemented in the dissipative controlled rocking connections of the Wigram-Magdala Link bridge in Christchurch, New Zealand in 2016. The research in this paper provides experimental testing and analytical modelling of grooved dissipaters. The dissipaters have been tested under quasi-static cyclic loading. Two types of analytical models, the Ramberg-Osgood and bilinear, have been used to model the behaviour of the dissipaters. It is shown that the Ramberg-Osgood model can capture the behaviour of the dissipater to an adequate level. Furthermore, the study discusses a simplified methodology to calculate the yield displacement of the dissipater, and the appropriate Ramberg-Osgood coefficient for simplified analytical modelling.

## 1 INTRODUCTION

Grooved dissipaters are metallic devices that can be used to dissipate seismic energy in bridge or building applications. Grooved dissipaters were originally developed and tested by (White 2014) at the University of Canterbury. The dissipaters were subsequently used in dissipative controlled rocking connections by (White 2014), (Mashal and Palermo 2014), (Mashal and Palermo, 2019), (White and Palermo 2016), and (Andisheh

et al. 2018). Grooved dissipaters offer advantages such as good ductility, strength, simple fabrication, cost-effectiveness, compact dimensions, and lightweight.

A typical grooved dissipater is made of a plain mild steel bar that is threaded at the ends, and has groove cuts in the middle region (Fig. 1). The bar is placed inside a confining tube which has a slightly larger inner diameter than the bar. The working concept of the dissipater under tension and compression loading is similar to that of Buckling-Restrained Braces (BRBs). During tension or compression axial loading, the dissipater yields at the grooved part. The outer-confining tube does not allow global buckling of the bar under compression. Grooved dissipaters can be made with two, three, or four cuts in the bar. Experimental investigation by (White 2014) suggested that the best performance results can be expected from a dissipater with three grooves. The study also suggested that it is necessary to leave a solid portion of the plain bar between the threaded and grooved parts to prevent premature failure of the dissipater under cyclic loading.

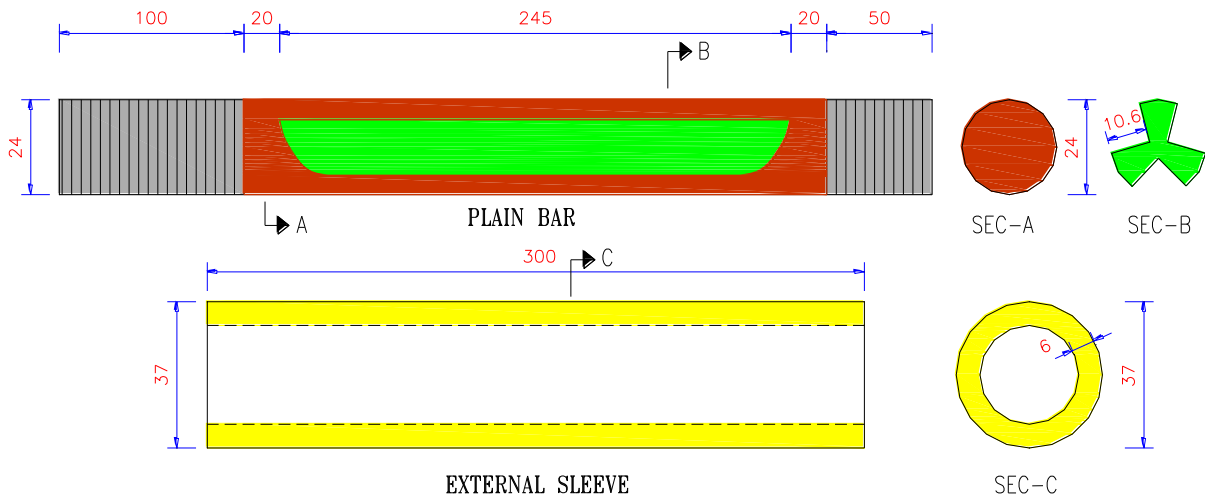


Figure 1: Grooved dissipater details (dimensions in mm)

Grooved dissipaters were implemented in the dissipative controlled rocking connections of the Wigram-Magdala Link bridge in Christchurch in 2016. The dissipaters are located at the column-to-footing and column-to-cap beam connections. During the 2016 Kaikoura earthquake, the bridge remained intact. This was not a particularly demanding earthquake since the ground shaking experienced in Christchurch was quite low. However, the bridge could be expected to behave very well under large earthquakes.



Figure 2: Wigram-Magdala Link bridge in Christchurch, New Zealand (courtesy of Jeremy Kelleher)

## 2 EXPERIMENTAL TESTING

Two grooved dissipaters were fabricated for quasi-static cyclic testing. One specimen (GD-1) was tested under net positive displacement, while the other one (GD-2) was tested under net positive and negative displacement. The dimensions were identical for both dissipaters. All dissipater parts (grooved bar and confining tube) were made of mild steel with yield strength of 350 MPa. The diameter of the solid bar was 24 mm. Three grooves each with a depth of 10.6 mm were cut into the solid bar. This gave a reduced sectional area of 203 mm<sup>2</sup> for the dissipater. The confining tube wall thickness was taken to be 6 mm. The grooved length of the dissipaters was selected such to limit the peak strain in the bar to 5% or lower under displacement levels of 10 mm and 6 mm (assumed to be ultimate state “ULS”) for GD-1 and GD-2, respectively. The maximum considered earthquake (MCE) displacements were assumed to be 20 mm and 10 mm, for GD-1 and GD-2, respectively. The reason behind targeting two different displacement levels was that GD-2 is subjected to a more demanding loading (both positive and negative displacements) which normally does not occur in dissipative rocking connection (Figure 4b).

Using basic engineering mechanics, the capacity of the dissipaters was estimated to be 71 kN at the yield point. Assuming an overstrength factor of 1.3, the capacity of GD-1 was estimated to be 92 kN at the maximum displacement under net positive deformation. Given the similarity of the grooved dissipaters to those studied by (Amaris Mesa 2010) and (Sarti et al. 2013), the capacity of GD-2 was expected to increase by a factor of 2 in compression. This means, the capacity of GD-2 under maximum net negative strain was estimated to be about 150 kN. Figure 1 presents dimensions and details of the dissipaters.

Testing arrangement was similar to that conducted by (Sarti et al. 2013) as shown in Figure 3b. The dissipaters were tested under axial loading under the 10MN DARTEC machine at the University of Canterbury. During testing, the axial force and displacement were monitored for each dissipater until the fracture point. Loading protocol for each dissipater was cyclic quasi-static and is shown in Figure 4.

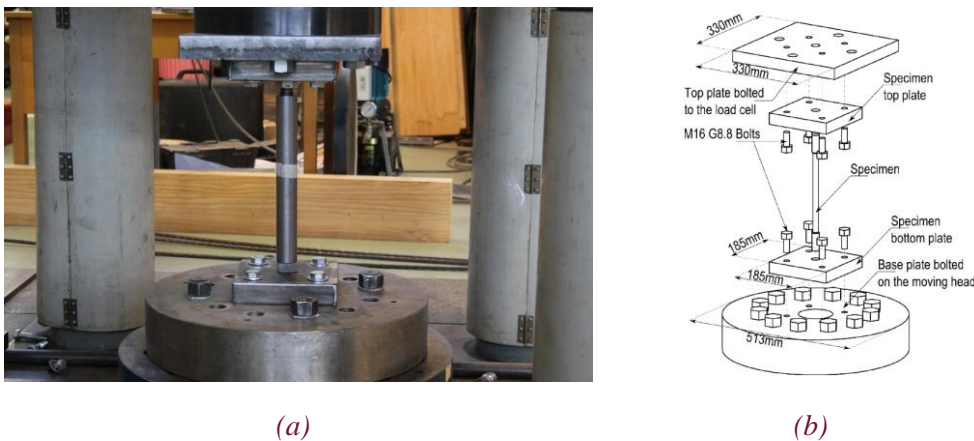


Figure 3: (a) Dissipater under testing, (b) testing setup (Sarti et al. 2013)

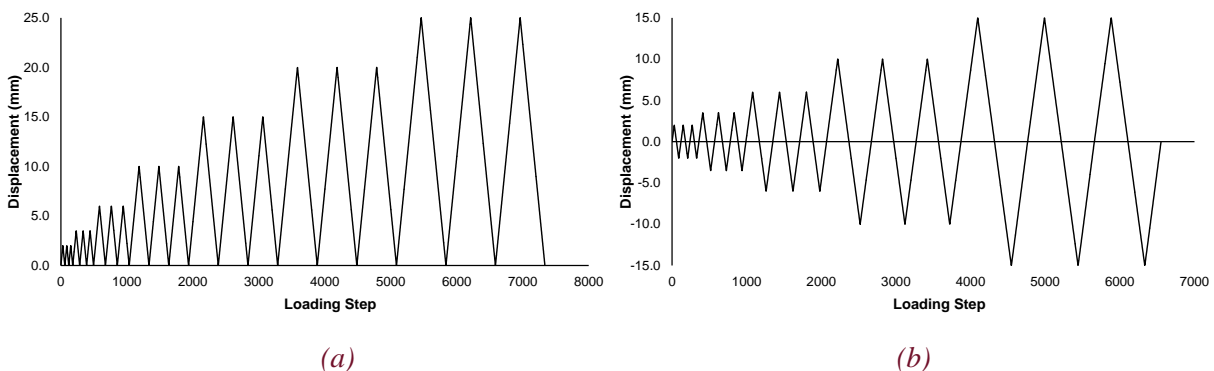


Figure 4: (a) Loading protocol for GD-1, (b) loading protocol for GD-2

## 2.1 Testing Results

Testing results for GD-1 showed that the dissipater completed all loading cycles up until cycles of 25 mm displacement. The dissipater fractured during the second cycle of 25 mm displacement. The fracturing cause was due to strength degradation and local buckling under cycles of high strains. Upon conclusion of the testing, evidence of snake-shape local buckling along the grooved length of the dissipater was noticed (Fig. 5). Testing results for GD-2 showed that the dissipater reached maximum displacement of 15 mm under net negative strain, but fractured as the dissipater was loaded to a similar displacement under net positive (tension) strain. The fracture was thought to be due to low-cycle fatigue and local buckling along the grooved length. The local buckling in GD-2 was more obvious and severe (Fig. 5b) than what observed in testing of GD-1 (Fig 5a).



Figure 5: Snake-shape local buckling and fracture of grooved dissipaters (a) GD-1, (b) GD-2

The axial force-displacement hysteresis for GD-1 under net positive strain is plotted in Figure 6a. The dissipater showed a stable hysteresis. The backbone curve is shown in Figure 6b. Considering the lower yield point on the backbone curve, the dissipater yielded at approximately 0.8% drift ratio or 3.5 mm. The drift ratio was calculated by dividing displacements to overall length of the dissipater (435 mm). GD-1 achieved a maximum capacity of just less than 100 kN in tension, and approximately a capacity of 150 kN in compression during the first cycle of 25 mm displacement (5.7% drift ratio). The ductility at the maximum displacement ( $\mu_{max}$ ) was 7.1. The residual displacement in the dissipater following the first cycle of 5.7% drift ratio was in order of 23.7 mm (5.45% drift ratio) which corresponded to 95% of the 5.7% drift ratio.

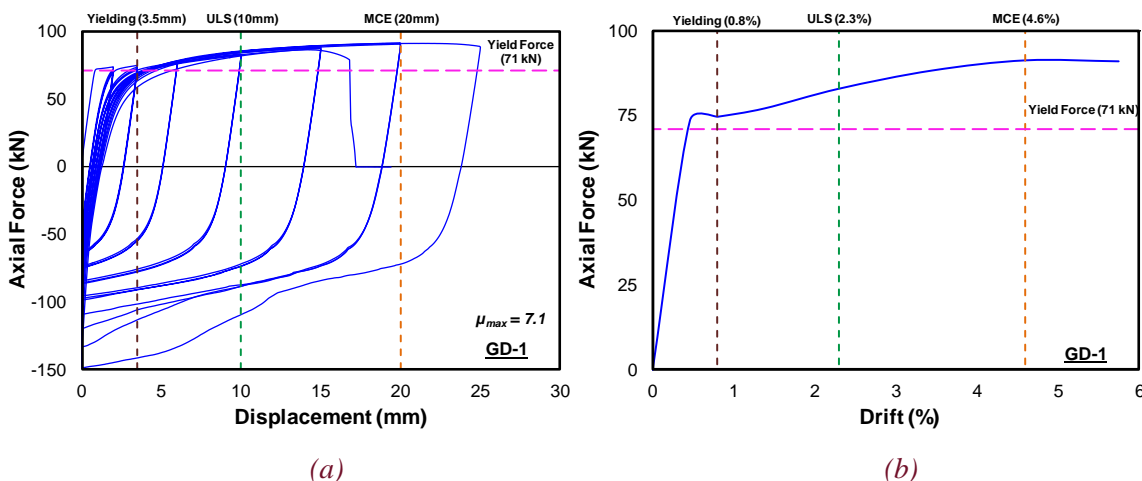
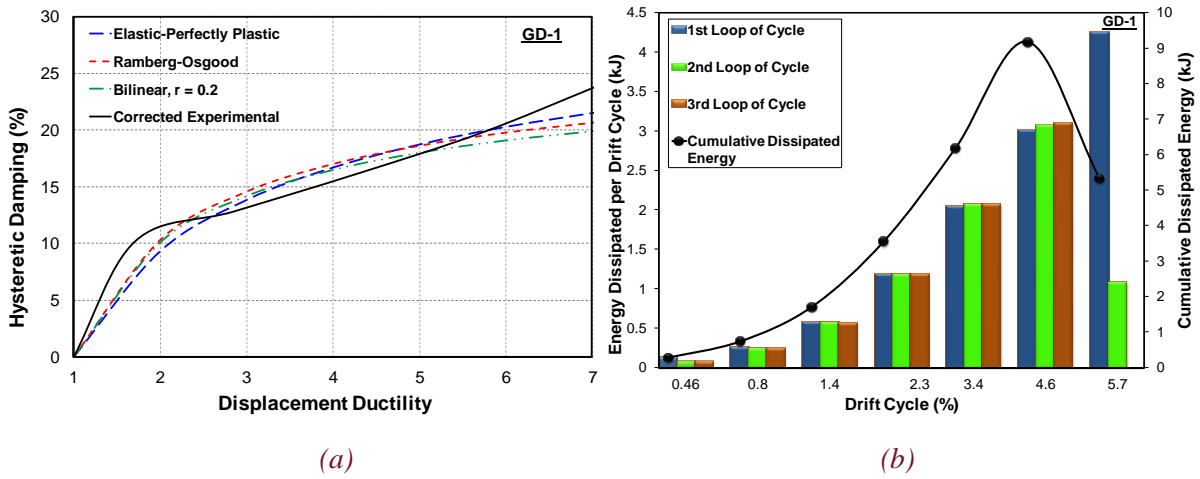


Figure 6: Testing results for GD-1 (a) force-displacement hysteresis, (b) backbone curve

The experimental hysteretic damping curve for GD-1 is plotted in Figure 7a in accordance with (Priestley et al. 2007). For ductility values of 1 up to 2.5, the hysteretic damping values for the dissipater were above those from existing theoretical models for elastic-perfectly plastic, Ramberg-Osgood, and bilinear ( $r = 0.2$ ). For ductility values of 2.5 up to 5.5, the values for hysteretic damping were just under the theoretical models. For ductility beyond 5.5, the hysteretic damping values were above the theoretical models up to the fracturing point. GD-1 attained a maximum hysteretic damping value of 24% at ductility of 7.1 during first cycle at maximum drift ratio of 5.7% (25 mm displacement). The energy dissipated per each cycle of each drift ratio for GD-1 derived from the experimental results is presented in Figure 7b. The cumulative dissipated energy in this figure is plotted by summing up the energy dissipated per each drift ratio.

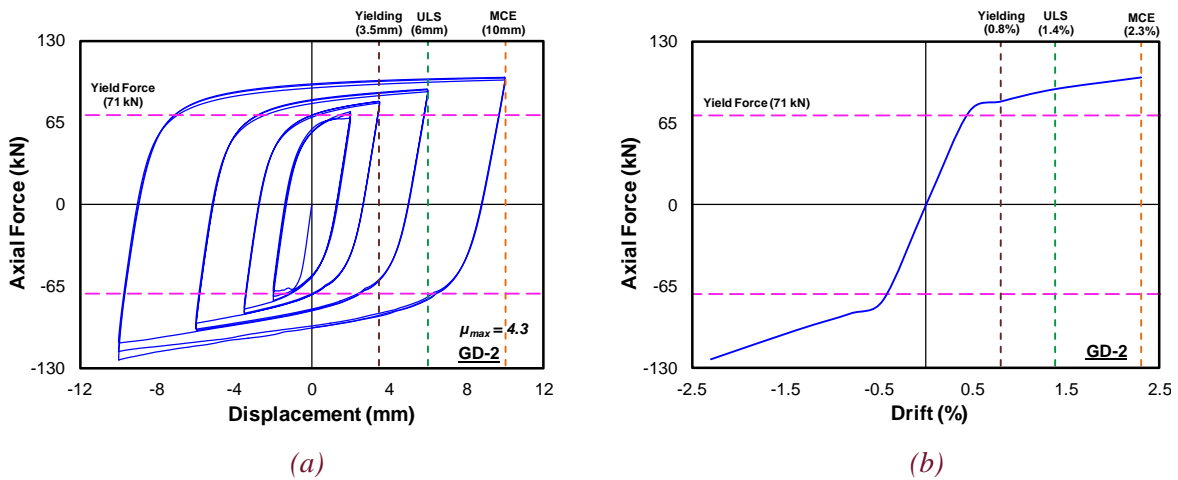


(a)

(b)

Figure 7: Testing results for GD-1 (a) Corrected area-based hysteretic damping, (b) dissipated energy

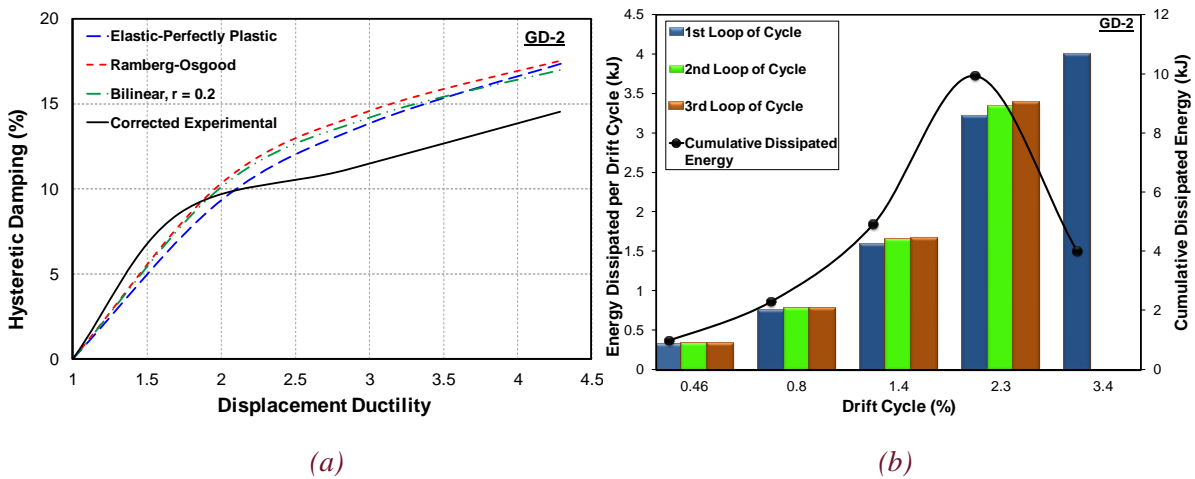
For GD-2, the axial force-displacement and backbone plots are presented in Figure 8. The yield point of the dissipater was similar to that of GD-1 (0.8% drift ratio). The dissipater showed a stable response with a slight increase in strength under net negative displacement (compression). The hysteretic damping trend versus theoretical models was similar to GD-1. Figures 9-10 present plots for hysteretic damping and dissipated energy for GD-2.



(a)

(b)

Figure 8: Testing results for GD-2 (a) force-displacement hysteresis, (b) backbone curve



(a)

(b)

Figure 9: Testing results for GD-2 (a) corrected area-based hysteretic damping, (b) dissipated energy

### 3 ANALYTICAL MODELLING

Simplified macro-analytical models such as Ramberg-Osgood (Ramberg and Osgood 1943) and bilinear (Naeim and Kelly 1999) were used to simulate the backbone curve and cyclic response of grooved dissipaters. The Ramberg-Osgood and bilinear hysteretic rules are illustrated in Figure 10. Both models incorporate balanced hysteresis in tension and compression stages of the loading.

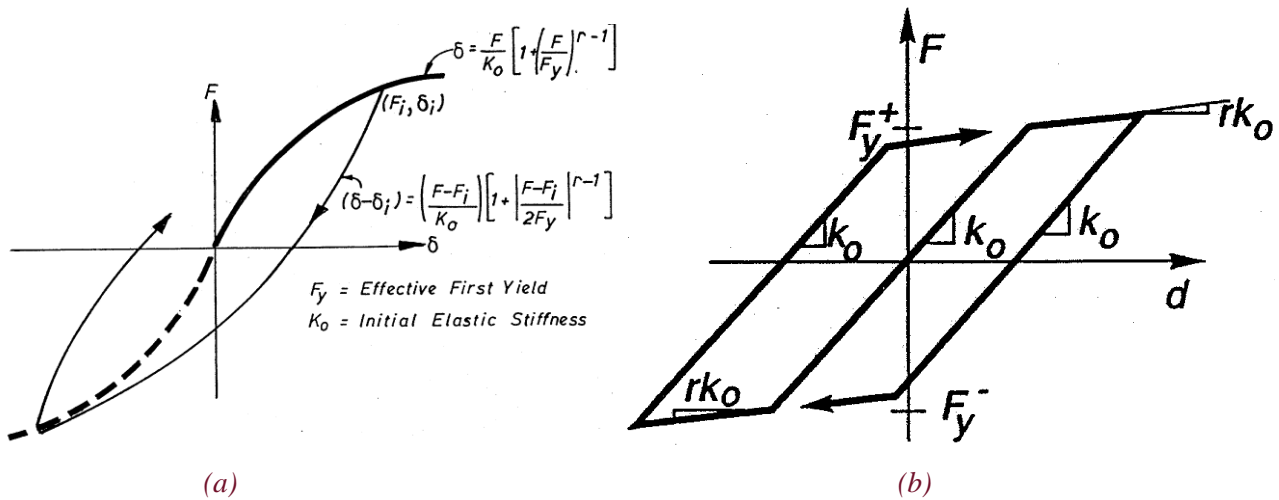


Figure 10: Hysteretic rules (a) Ramberg-Osgood, (b) bilinear (Carr, 2005)

Traditionally, the Ramberg-Osgood model has been used to model the cyclic response of structural steel members. In this model, one of the most important parameters is the ( $r$ ) coefficient. For a linear elastic system  $r = 1.0$ . With increasing values of ( $r$ ), the post-yield stiffness of the system is decreasing. This means that with  $r = \infty$ , the response of the system would be that of elastic-perfectly plastic model.

The bilinear hysteretic model was originally developed to capture the dynamic behaviour of a system that incorporates isolation devices, in particular the friction pendulums. However, this model can also be utilized as a simplified tool for modelling the response of metallic dissipaters such as grooved dissipaters.

In simplified analytical modelling of grooved dissipaters, the initial stiffness of the dissipater is important to be considered. The initial stiffness can be calculated by using a similar procedure to that presented in (Sarti et al. 2013) for modelling the response of Buckling-Restrained Fused Type (BRF) dissipater. In this approach when calculating the initial stiffness of the dissipater, the influence of the elastic deformation over the non-yielding portions of the dissipater are taken into account. Figure 11 presents geometrical parameters for grooved dissipaters.

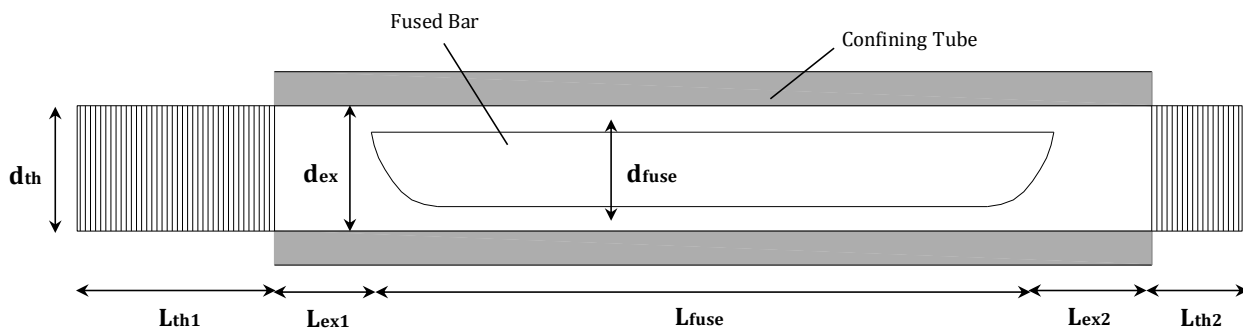


Figure 11: General geometrical parameters for grooved dissipaters

Using the procedure from Sarti et al. (2013), the yield displacement ( $\Delta_Y$ ) can be calculated from Equation 1.

$$\Delta_Y = \frac{\sigma_y A_{fuse} L_{ex1}}{E A_{ex1}} + \frac{\sigma_y A_{fuse} L_{fuse}}{E A_{fuse}} + \frac{\sigma_y A_{fuse} L_{ex2}}{E A_{ex2}} + \frac{\sigma_y A_{fuse} L_{th1}}{E A_{th1}} + \frac{\sigma_y A_{fuse} L_{th2}}{E A_{th2}} \quad (1)$$

In most cases,  $A_{ex1} = A_{ex2}$  and  $A_{th1} = A_{th2}$ . Therefore, an identical value of  $A_{ex}$  and  $A_{th}$  can be used and Equation 1 can be re-written as follows:

$$\Delta_Y = \frac{\sigma_y A_{fuse} (L_{ex1} + L_{ex2})}{E A_{ex}} + \frac{\sigma_y L_{fuse}}{E} + \frac{\sigma_y A_{fuse} (L_{th1} + L_{th2})}{E A_{th}} \quad (2)$$

Using  $L_{ex} = L_{ex1} + L_{ex2}$ ,  $L_{th} = L_{th1} + L_{th2}$ ,  $A_{fuse} = (\pi/4) d_{fuse}^2$ ,  $A_{ex} = (\pi/4) d_{ex}^2$  and  $A_{th} = (\pi/4) d_{th}^2$ , Equation 2 can be re-written as:

$$\Delta_Y = \frac{\sigma_y L_{fuse}}{E} \left[ \left( \frac{d_{fuse}}{d_{ex}} \right)^2 \frac{L_{ex}}{L_{fuse}} + 1 + \left( \frac{d_{fuse}}{d_{th}} \right)^2 \frac{L_{th}}{L_{fuse}} \right] \quad (3)$$

Generally  $A_{th} \approx 0.75 A_{ex}$  which gives  $d_{th} \approx 0.866 d_{ex}$ . The maximum stress ( $\sigma_u$ ) in the dissipater under cyclic loading can be taken as 1.3 times of the yield stress ( $\sigma_y$ ). This means that the ultimate force ( $F_U$ ) in the dissipater under net positive deformation would be approximately 1.3 times the yield force ( $F_Y$ ).

To calculate the Ramberg-Osgood coefficient ( $r$ ), a rupturing strain ( $\varepsilon_r$ ) of 10% can be assumed for the dissipater under cyclic loading at MCE level. Using Equations 4 and 5, the Ramberg-Osgood coefficient ( $r$ ) can be calculated in accordance with ‘‘Metallic Materials Properties Development and Standardization’’ (MMPDS-01 2003). The value of  $r$  was calculated to be approximately 15 for grooved dissipaters.

$$r = \frac{\ln \left( \frac{\varepsilon_{us}}{0.2} \right)}{\ln \left( \frac{\sigma_u}{\sigma_y} \right)} \quad (4)$$

$$\varepsilon_{us} = 100 \left( \varepsilon_r - \frac{\sigma_u}{E} \right) \quad (5)$$

In Equations 4 and 5,  $\varepsilon_{us}$  is the uniform strain which can be defined as the plastic strain at the end of uniform elongation at the maximum tensile load.

In this research, analytical models were developed for GD-1 which was tested under net positive deformation only. The modelling procedure for GD-2 will be similar to what is for GD-1. Utilizing Equation 1 through Equation 5, Table 1 presents a summary of the modelling parameters for GD-1.

*Table 1: Summary of modelling parameters for GD-1.*

$\Delta_Y = 0.14\%$	$d_{bar} = 24 \text{ mm}$	$L_{bar} = 435 \text{ mm}$	$\sigma_y = 350 \text{ MPa}$	$\varepsilon_y = 0.175\%$
$\Delta_U = 5.75\%$	$d_{fuse} = 16 \text{ mm}$	$L_{fuse} = 245 \text{ mm}$	$\sigma_u = 455 \text{ MPa}$	$\varepsilon_r = 10\%$
$F_Y = 70.4 \text{ kN}$	$d_{ex} = 24 \text{ mm}$	$L_{ex} = 40 \text{ mm}$	$E = 200,000 \text{ MPa}$	$\varepsilon_{us} = 9.77\%$
$F_U = 91.5 \text{ kN}$	$d_{th} = 20.8 \text{ mm}$	$L_{th} = 150 \text{ mm}$	$K_0 = 114.35 \text{ kN/mm}$	$r = 15$

Figure 12 presents comparison of experimental and analytical plots for GD-1. It can be observed that the bilinear model predicts the initial stiffness of the dissipater slightly better than the Ramberg-Osgood model

(Fig. 12b). However, for an overall behaviour, the Ramberg-Osgood model provides better results (Fig. 12a). The deviation in elastic stiffness of the dissipater from comparison of experimental results versus analytical models in Figure 12, can be a result of flexibility and slack in the end connections of the dissipater during testing.

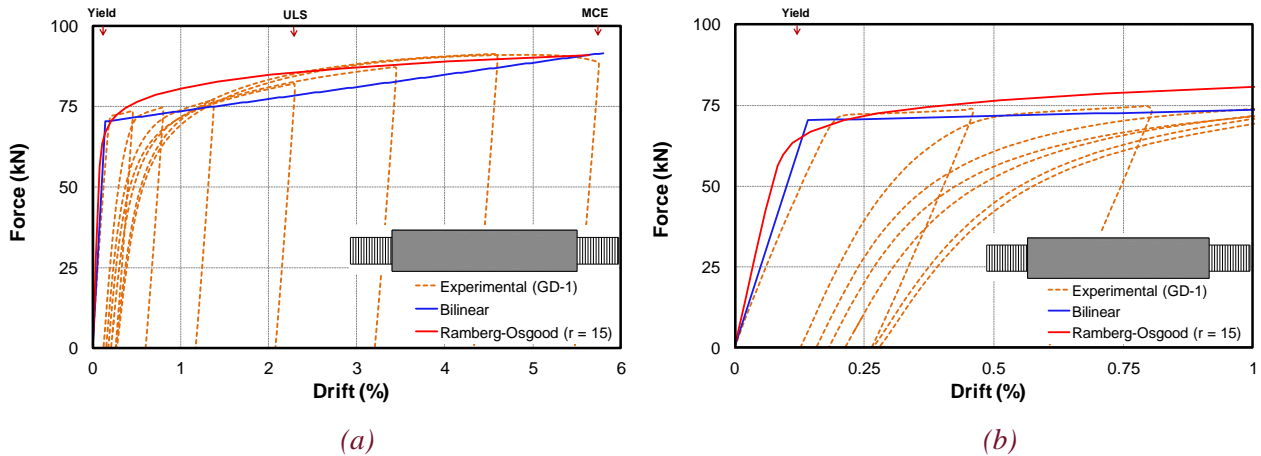


Figure 12: Analytical backbone models for GD-1 (a) overall backbone curve, (b) close-up of initial stiffness

The force-drift hysteresis plots for Ramberg-Osgood and bilinear models are shown in Figure 13. It can be noticed that the Ramberg-Osgood model (Fig. 13a) provides a better analytical model for the dissipater. The bilinear model (Fig. 13b) also captures the cyclic response of the dissipater to an adequate level.

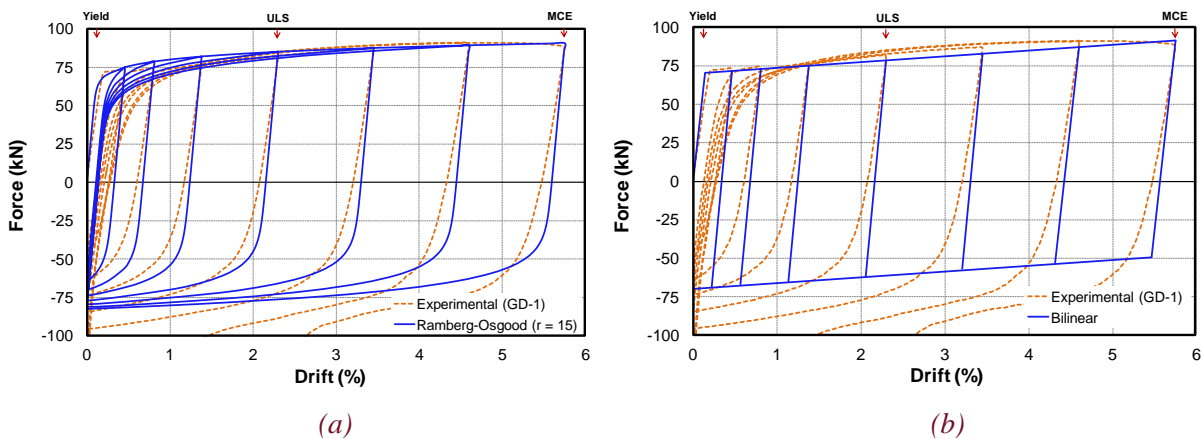


Figure 13: Analytical force-drift hysteresis for GD-1 (a) Ramberg-Osgood, (b) bilinear

## 4 CONCLUSIONS

Grooved dissipaters offer good advantages such as higher capacity in a smaller package, easy fabrication, and good energy dissipation. Experimental testing in this research investigated the response of grooved dissipaters under quasi-static loading.

Two identical specimens were developed and tested. One dissipater (GD-1) was tested under net positive (tension) displacement while the other one was tested under both net positive and negative displacement. The loading protocol for GD-1 represented a case similar to what can be expected of external dissipaters in a dissipative controlled rocking connection. GD-1 achieved its predicted capacity and maximum displacement ductility of 7.1 before fracturing in low-cycle fatigue during the second cycle of 5.7% drift ratio which corresponded to 25 mm displacement. The maximum drift ratio for which the dissipater could complete all three cycles was at maximum considered level loading was 4.6% drift ratio or 20 mm displacement. The corrected experimental damping curve suggested that the dissipater reached maximum hysteretic damping of

24% before the failure. This was slightly higher than those obtained from theoretical models such as Ramberg-Osgood, elastic-perfectly plastic, and bilinear with ( $r = 0.2$ ).

For GD-2, the specimen was subjected to positive (tension) and negative (compression) displacement which is a more demanding loading protocol. This type of loading can represent a scenario where the dissipater is used as a brace. GD-2 showed a stable hysteresis with similar response to that of GD-1. There was a slight increase (22%) in the strength of the dissipater under compression during cycles of maximum considered earthquake level drift ratio (2.3% drift ratio or 10 mm displacement). GD-2 achieved a maximum ductility of 4.3 before fracturing in low-cycle fatigue during the first cycle of 3.4% drift ratio which corresponded to 15 mm displacement. The corrected experimental damping values were slightly lower than those observed in testing of GD-1 because of lower levels of displacement. Before fracturing in low-cycle fatigue, the dissipater attained a maximum hysteretic damping of 14%. Observations from testing showed larger snake-shape local buckling in the grooved portion of the dissipater in GD-2 compared to GD-1.

The research showed that simplified analytical models such as Ramberg-Osgood and bilinear can be used to predict the monotonic and cyclic response of grooved dissipaters. When calculating the initial stiffness of the dissipater, the influence of elastic deformation over the non-yielding parts (solid part of the bar, threaded lengths, etc.) of the bar should be considered for better results. The maximum force in grooved dissipaters under net positive deformation can be approximated to be 1.3 times the yield force. This value was about 2.0 for grooved dissipaters under net positive and negative deformation. Precise machining is thought to improve the overstrength factor for grooved dissipaters.

For the Ramberg-Osgood model, the coefficient ( $r$ ) can be taken as 15 for grooved dissipaters made of mild steel bars under net positive deformation. During testing, it is thought that flexibility and stretch in the end connections and non-yielding part of the dissipater played a role in reducing the initial stiffness. While the Ramberg-Osgood and bilinear models took into account the elastic deformation over the non-yielding parts, however both models slightly over predicted the elastic stiffness of the dissipater. The bilinear model provided better results for the elastic stiffness compared to Ramberg-Osgood model. For modelling the overall hysteretic response of the dissipater, the Ramberg-Osgood model provided better results compared to bilinear model. Further experimental and analytical research is recommended to refine the existing theoretical models for predication of the response of grooved dissipaters. In this regard, effects such as the depth and type of threaded ends, variation in the depth of the grooved cuts, material properties of the bar, local buckling of the bar under compression, influence of the gap between the bar and the confining tube, and the friction between the inner surface of the confining tube and the grooved bar during compression, should be explored.

## 5 ACKNOWLEDGEMENTS

The authors are thankful of technicians John Maley and Gavin Keats for their help with fabrication and testing of the dissipaters.

## 6 REFERENCES

- Amaris-Mesa, D.A. 2010. *Developments of Advanced Solutions for Seismic Resisting Precast Concrete Frames*, PhD Thesis, University of Canterbury, Christchurch, New Zealand.
- Andisheh, K., Liu, R., Palermo, A. & Scott, A. 2018. Cyclic Behavior of Corroded Fuse-Type Dissipaters for Posttensioned Rocking Bridges, *Journal of Bridge Engineering*.
- Mashal, M., Palermo, A. & K.G. 2019. Innovative dissipaters for earthquake protection of structural and non-structural components, *Soils Dynamics and Earthquake Engineering*, Vol 116 31–42.
- Mashal, M., White, S. & Palermo, A. 2014. Accelerated bridge construction and seismic low-damage technologies for short-medium span bridges, *37th IABSE Symposium on Engineering for Progress, Nature and People*, 1208–1215.

- MMPDS-01. 2003. *Metallic Materials Properties Development and Standardization (MMPDS)*, Department of Transportation, Washington, D.C., United States.
- Naeim, F. & Kelly, J.M. 2000. Design of Seismic Isolated Structures: From Theory to Practice, *Earthquake Spectra*, Vol 16(3) 709–710.
- Priestley, M.J.N., Calvi, G.M. & Kowalsky, M.J. 2007. *Displacement-based seismic design of structures*.
- Ramberg, W. & Osgood, W.R. 1943. *Description of stress-strain curves by three parameters*, National Advisory Committee For Aeronautics, Technical Note No. 902.
- Sarti, F., Smith, T., Palermo, A., Pampanin, S., Bonardi, D. & Carradine, D.M. 2013. Experimental and analytical study of replaceable Buckling-Restrained Fuse-type (BRF) mild steel dissipaters, *2013 NZSEE Conference*, 8.
- White, S. 2014. *Controlled damage rocking systems for accelerated bridge construction*, Masters Thesis, University of Canterbury, Christchurch, New Zealand.
- White, S. & Palermo, A. 2016. Quasi-Static Testing of Posttensioned Nonemulative Column-Footing Connections for Bridge Piers, *Journal of Bridge Engineering*.